ChemComm

COMMUNICATION

View Article Online
View Journal | View Issue

Cite this: *Chem. Commun.*, 2019, **55**, 8138

Received 14th May 2019,
Accepted 13th June 2019

DOI: 10.1039/c9cc03705e

rsc.li/chemcomm

Photoreaction-driven two-dimensional periodic polyrotaxane-type supramolecular nanoarchitecture†

Cai-Cai Zhang,[a] Ying-Ming Zhang,[a] Zhi-Yuan Zhang,[a] Xuan Wu,[a] Qilin Yu[a] and Yu Liu *[ab]

A 2D polypseudorotaxane-type assembly was constructed using cucurbit[8]uril and styrylpyridinium-bearing triphenylamine. In addition, tunable non-covalent to covalent transition was achieved by [2+2] photodimerization of styrylpyridinium units. Thus, a more stable 2D polyrotaxane-type nanoarchitecture was obtained, which could capture [60]fullerene and further exhibit an excellent photodynamic therapy effect.

Two-dimensional (2D) nanostructures have been utilized as a significant class of materials with diverse promising applications.[1] Currently, some successful bottom-up strategies for the construction of 2D nanosheets are mainly dependent on the self-assembly of organic small molecules *via* multiple interactions, such as metal–ligand coordination, hydrogen-bonding interconnection, and dynamic chemical bonds.[2] In this regard, macrocycle-based supramolecular methods provide more opportunities to fabricate various 2D nanostructures with structural and functional diversity.[3] For example, Li and co-workers presented a 2D supramolecular organic framework, in which cucurbituril was used as rigidified macrocycle to stabilize the dimers of aromatic components through host–guest interactions.[4] Our group also reported a supramolecular 2D nanoassembly system *via* the supramolecular assembly of adamantyl diphenylalanine with azobenzene-bridged bis(β-cyclodextrin), thus displaying photocontrolled morphological interconversion from 1D nanotubes to 2D nanosheets.[5]

Despite the recent remarkable progress in developing macrocycle-based 2D supramolecular assemblies, the commonly used strategies are achieved based on complex- or pseudorotaxane-type structures, which may result in the undesirable structural instability and eventually impede their practical applications. With this in mind, we herein report a convenient approach to construct a porous and stable 2D supramolecular assembly through photoreaction-driven transformation from pseudorotaxane to rotaxane, which can synergistically combine the immense advantages of desirable controllability from noncovalent complexation and high stability from a covalently bonded molecular skeleton (Scheme 1).

In our case, a paddle-shape triphenylamine bearing styrylpyridinium unit (TPA-SP) was synthetized, which could form layered a polypseudorotaxane-type nanostructure upon inclusion complexation with cucurbit[8]uril (TPA-SP⊂CB[8]). More interestingly, the obtained TPA-SP⊂CB[8] assembly could be readily transformed to a more stable 2D periodic polyrotaxane-type nanostructure

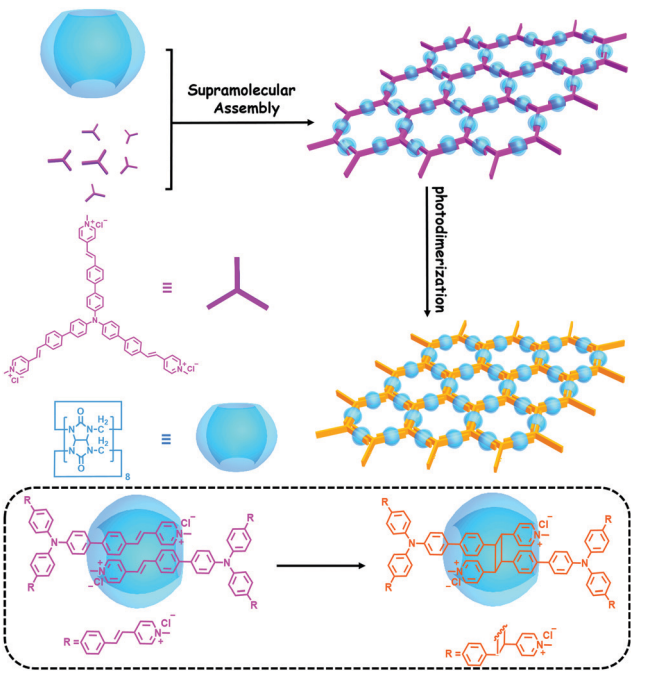

Scheme 1 Schematic illustration of the formation of a 2D periodic polyrotaxane-type nanostructure in water.

[a] *Department of Chemistry, State Key Laboratory of Elemento-Organic Chemistry, Nankai University, Tianjin 300071, P. R. China*

[b] *Collaborative Innovation Center of Chemical Science and Engineering (Tianjin), Tianjin 300072, China. E-mail: yuliu@nankai.edu.cn*

† Electronic supplementary information (ESI) available: Detailed synthesis, characterization data, Job's plots, association constants, absorption spectra and transmission electron microscopy images. See DOI: 10.1039/c9cc03705e

(TPA-SP$_{PD}$⊂CB[8], 'PD' denotes photodimerization) *via* the macrocycle-assisted [2+2] photodimerization of styrylpyridinium units under visible light irradiation. Furthermore, the well-defined TPA-SP$_{PD}$⊂CB[8] nanosheets could efficiently capture [60]fullerene in water, thus presenting an excellent DNA cleavage ability and photodynamic therapy effect arising from the photoinduced generation of reactive oxygen species. To the best of our knowledge, the TPA-SP$_{PD}$⊂CB[8] assembly is one of the rarely reported photoreaction-driven 2D free-standing nanoarchitectures consisting of periodic polyrotaxanes in water.

There are two structural features of our designed TPA-SP as the guest molecule: (1) the TPA core presented a three-bladed propeller structure, which can effectively prevent the undesirable intermolecular aggregation[6] and (2) the peripheral styrylpyridinium (SP) units not only play the role of anchoring points to bind with CB[8] at a molar ratio of 2 : 1 in a head-to-tail stacking pattern, but also act as the active sites for the intermolecular cross-linking in photochemical reactions.

First, the molecular binding behaviors between CB[8] and TPA-SP were investigated. The proton signals of TPA-SP in D_2O alone were indistinguishable due to its long-range and rotatable molecular skeleton (Fig. S12b, ESI†). Unexpectedly, the proton signals became identifiable and clear upon gradual addition of CB[8]. All the proton signals of TPA-SP reached the equilibrium state with 1.5 equiv. CB[8] and no obvious chemical change was observed in the presence of excess CB[8] (Fig. S12c–e, ESI†). The Job's plot further confirmed that the binding stoichiometry was 2 : 3 in the TPA-SP⊂CB[8] complexation (Fig. S13, ESI†). Moreover, UV/vis spectroscopic titration quantitatively revealed the high association constants between TPA-SP and CB[8] (Fig. S14, ESI†). Accordingly, the dynamic light scattering (DLS) data also showed that the average hydrodynamic diameter of the TPA-SP⊂CB[8] assembly was 269 nm, indicative of the existence of a large-sized supramolecular assembly in water (Fig. S15, ESI†).

To shed more light on the binding mechanism between TPA-SP units and CB[8], a model compound M-SP with a single arm was synthetized as described in Scheme S2 (ESI†). ^{1}H NMR titrations were further conducted to investigate the host–guest complexation of M-SP with CB[8]. As discerned from Fig. S17d (ESI†), all the proton signals of M-SP displayed upfield shifts upon addition of 0.5 equiv. CB[8]. Moreover, the 2D NOESY spectrum revealed that the two M-SP units were simultaneously immersed in the cavity of CB[8] in a head-to-tail stacking pattern, which was propitious for the photodimerization of two adjacent SP units (Fig. S19, ESI†).

With these results in mind, we next investigated the formation of polypseudorotaxane mediated by two SP units in the CB[8] cavity. Transmission electron microscopy (TEM), scanning electron microscopy (SEM), and atomic force microscopy (AFM) were employed to characterize the morphology of the TPA-SP⊂CB[8] assembly. As shown in Fig. 1, layered graphene-like structures were observed in the TEM image, and the thickness of the obtained nanosheets was investigated *via* the tapping-mode AFM experiments, presenting a uniform height of approximately 1.91 nm, corresponding to the outer

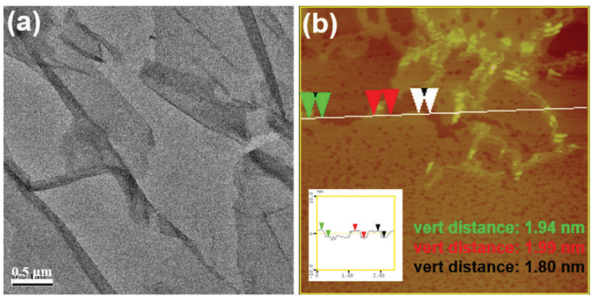

Fig. 1 (a) TEM image and (b) tapping-mode AFM image of the 2D TPA-SP⊂CB[8] assembly.

diameter of CB[8].[7] Moreover, similar 2D nanosheets were also observed in the SEM images (Fig. S21, ESI†). These experimental results indicated that a single-layer 2D supramolecular assembly was constructed by TPA-SP⊂CB[8] complexation. To further explore the structural information, a grazing incidence small angle X-ray scattering (GI-SAXS) experiment was performed for the solid sample of the TPA-SP⊂CB[8] assembly. A sharp peak at a spacing of 3.8 nm, which was consistent with the simulated pore diameter of 3.9 nm, appeared in the small angle region (Fig. S22, ESI†). In addition, the Brunauer–Emmett–Teller (BET) surface area of the TPA-SP⊂CB[8] assembly was identified as 38 $m^2\ g^{-1}$, which was a relatively small value due to the ultrathin layered structure (Fig. S23, ESI†). Thermogravimetric analysis (TGA) showed that TPA-SP⊂CB[8] revealed good thermal stability (Fig. S24, ESI†).

It is well-known that there are three main types of stilbazolium-involved photoreactions, *i.e.* photoisomerization, photocyclization and photodimerization, which have attracted much attention in the construction of various photoresponsive nanosystems.[8] In our case, two SP units were co-included in the cavity of CB[8] with a head-to-tail pattern, which is favorable for the photodimerization reaction. Thus, the photoreaction properties of M-SP were explored (Fig. S25–S27, ESI†). Compared to the photoreaction of M-SP alone with both photoisomerization and photodimerization behaviors, the conversion of photodimerization was obviously improved upon addition of CB[8]. Therefore, it seems that CB[8] could not only act as the host molecule for the formation of a 1 : 2 complex but also offer a catalytic environment for the photodimerization of SP units at the same time.[9] In addition, the pK_a value of the TPA-SP⊂CB[8] system was also determined before light irradiation (Fig. S28, ESI†).[10] After analysis of the absorbance *versus* pH value, no obvious change was observed in the titration curve before and after addition of CB[8] to the TPA-SP solution, suggesting that the protonation site was virtually unaffected by CB[8]. Moreover, to investigate the stability of the supramolecular assembly, the Job's plot and association constant were explored in 50 mM glycine–hydrochloric acid buffer (pH = 2.2). No change in either binding stoichiometry or stability constant was observed under the acidic conditions, implying the high stability of the TPA-SP⊂CB[8] assembly (Fig. S29 and S30, ESI†).

The photoreaction of TPA-SP⊂CB[8] was further examined in both the neutral state and acidic state (pH = 2.2).

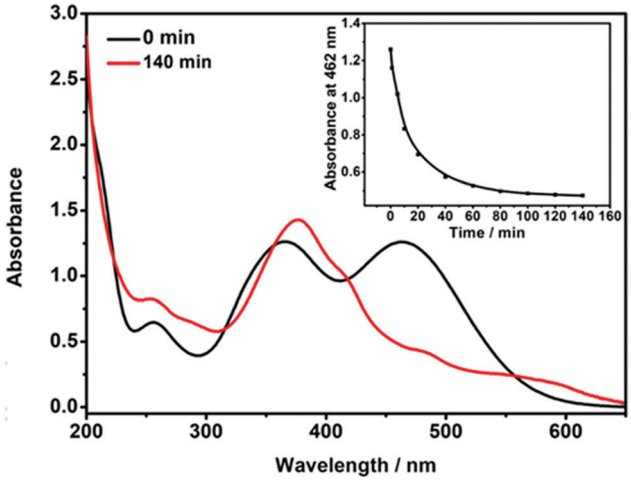

Fig. 2 UV/vis spectral change of TPA-SP⊂CB[8] (pH = 2.2) before and after light irradiation at 420 nm ([TPA-SP] = 0.2 mM, the light path was 1 mm. Inset: Absorbance change at 462 nm *versus* irradiation time).

No dramatic change was observed in the UV/vis spectra after irradiating the sample in the neutral state at 420 nm for 60 min, demonstrating that the SP units were almost not photodimerized because the triphenylamine unit in TPA-SP acted as an electron donating group which could form an intramolecular charge transfer state by photoexcitation and thus inhibit the photoreaction process (Fig. S31, ESI†).[11] In contrast, the absorbance at 462 nm decreased obviously in the acidic state corresponding to the photodimerized SP units, which was contributed to the protonation of the triphenylamine unit. As shown in Fig. 2, the photodimerization reaction was accelerated in the first 20 min and then virtualy completed in 60 min. After photodimerization was accomplished, the product was dialyzed for 24 hours to eliminate the unreacted substrates and excess hydrochloric acid. The Fourier transform infrared (FTIR) spectra of the freeze-drying sample of the TPA-SP_{PD}⊂CB[8] assembly presented a declining peak of the C=C stretching band at 1590 cm^{-1} and C=C–H out-of-plane bending bands at 992 and 828 cm^{-1}, which could be assigned to the vinylene group (Fig. S33, ESI†).[12]

More satisfactorily, the photodimerization product TPA-SP_{PD}⊂CB[8] was soluble and quite stable in water, benefiting from the protective effect of CB[8]. In addition, the size and morphology of the TPA-SP_{PD}⊂CB[8] assembly before and after light irradiation manifest that the graphene-like 2D structure was well conserved in DLS and SEM experiments (Fig. S34 and S35, ESI†). As shown in Fig. 3, the TEM and AFM experiments demonstrated a single-layer structure in the 2D periodic polyrotaxane-type TPA-SP_{PD}⊂CB[8] assembly. This well-defined nanostructure was further confirmed by GI-SAXS with sharp scattering peaks at 2θ = 2.47° and 4.17° (Fig. S36, ESI†). The corresponding pore diameter value of the TPA-SP_{PD}⊂CB[8] assembly (3.4 nm) was relatively smaller than that of TPA-SP⊂CB[8] (3.9 nm), because of the more rigidified structure after photodimerization. Furthermore, a competitive compound Ad-com with higher binding constant with CB[8] was

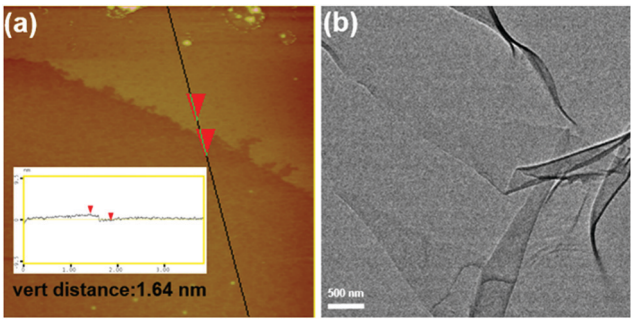

Fig. 3 (a) Tapping-mode AFM image and (b) TEM image of TPA-SP_{PD}⊂CB[8].

synthesized (Scheme S3, ESI†) and utilized to confirm the stability of TPA-SP_{PD}⊂CB[8] (Fig. S37, ESI†).[13]

After understanding the porous structure of the obtained TPA-SP_{PD}⊂CB[8] assembly, we next investigated its encapsulation properties toward guest molecules with an appropriate molecular size. As one kind of allotrope of carbon, [60]fullerene (C_{60}) is widely attractive for materials science and medicine application.[14] Therefore, the capture ability of TPA-SP_{PD}⊂CB[8] for C_{60} was studied in aqueous solution. In our case, the pristine C_{60} was added into the solution of TPA-SP_{PD}⊂CB[8] under ultrasonic conditions, and then the excess undissolved C_{60} was removed by centrifugation. The absorbance at 266 and 358 nm in the UV/vis spectra as well as the vibration bands at 524 and 573 cm^{-1} in the FTIR spectrum of C_{60}@(TPA-SP_{PD}⊂CB[8]) collectively suggested the formation of an advanced supramolecular assembly (Fig. S39 and S40, ESI†).[15] In contrast, TPA-SP⊂CB[8] exhibited a weaker ability to capture C_{60} through the same operation, due to the lack of compactness and stability (Fig. S41, ESI†). In addition, the BET value decreased from 35 $m^2\ g^{-1}$ for TPA-SP_{PD}⊂CB[8] to only 7 $m^2\ g^{-1}$, and the pore size distribution (Fig. S42 and S43, ESI†), as well as the TGA curve (Fig. S44, ESI†) changed before and after treatment of TPA-SP_{PD}⊂CB[8] with C_{60}.[16] Based on these experimental results, we speculated that the possible mode is that C_{60} molecules were encapsulated in the nanopores of TPA-SP_{PD}⊂CB[8].[17]

It is well-documented that C_{60} possesses an excellent DNA photocleavage ability due to the production of reactive oxygen species (ROS) under visible light irradiation.[18] Since C_{60}@(TPA-SP_{PD}⊂CB[8]) was highly water-soluble, agarose gel electrophoresis assay was performed to explore its potential application in photodynamic therapy.[19] Thus, pBR322 plasmid DNA was chosen to investigate the C_{60}@(TPA-SP_{PD}⊂CB[8]) cleavage ability. As shown in Fig. 4a, C_{60}@(TPA-SP_{PD}⊂CB[8]) displayed a concentration-dependent cleavage ability, and close supercoiled DNA (form I) was cleaved into nicked DNA (form II) by C_{60}@(TPA-SP_{PD}⊂CB[8]) at a concentration of 12 μM under white light irradiation for 30 min. Comparatively, the control experiments showed that C_{60}@(TPA-SP_{PD}⊂CB[8]) could not exhibit any DNA cleavage ability in the dark, suggesting that no ROS product was generated without light irradiation (lanes 7–13).

Furthermore, A549 cells (the human lung tumor cell lines, obtained from the cell Center of Peking Union Medical College)

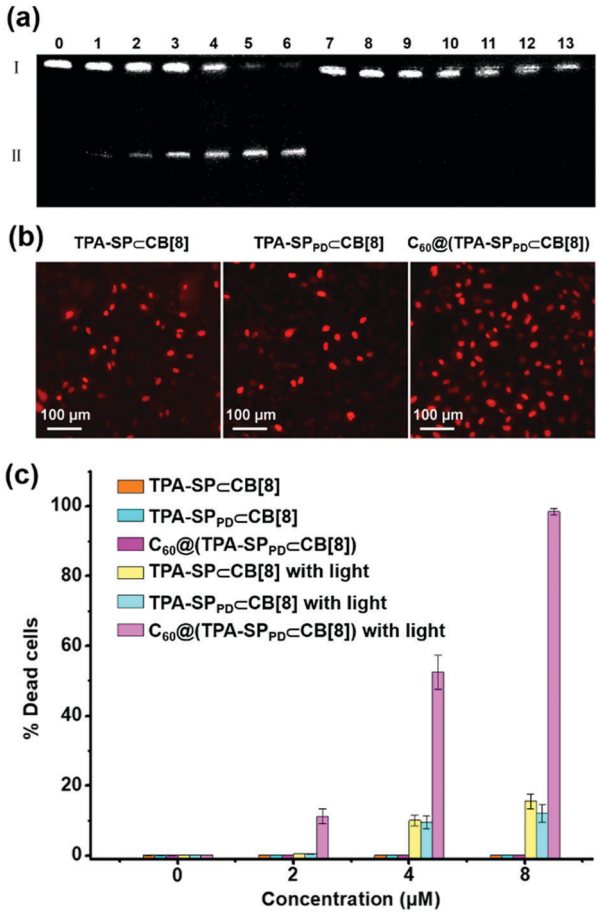

Fig. 4 (a) Agarose gel electrophoresis assay of pBR322 DNA (10 ng μL^{-1}) + C$_{60}$@(TPA-SP$_{PD}$⊂CB[8]) ([TPA-SP] = 0, 2, 4, 6, 8, 10, 12 μM, from lanes 0 to 6), upon white light irradiation for 30 min. Solutions with concentrations corresponding to 1–6 kept in the dark environment for lanes 7–13, respectively. (b) Confocal microscopy images of A549 cell lines after treatment with TPA-SP⊂CB[8], TPA-SP$_{PD}$⊂CB[8], and C$_{60}$@(TPA-SP$_{PD}$⊂CB[8]) ([TPA-SP] = 8 μM). Propidium iodide (PI) was used to stain the dead cells. (c) Cytotoxicity induced by the photodynamic activity of TPA-SP⊂CB[8], TPA-SP$_{PD}$⊂CB[8], and C$_{60}$@(TPA-SP$_{PD}$⊂CB[8]) at various concentrations with or without white light irradiation.

were employed to evaluate the photodynamic therapy potential of the C$_{60}$@(TPA-SP$_{PD}$⊂CB[8]) assembly. The cytotoxicity of TPA-SP⊂CB[8], TPA-SP$_{PD}$⊂CB[8], and C$_{60}$@(TPA-SP$_{PD}$⊂CB[8]) assemblies was comparatively studied (Fig. 4b and c). That is, in the dark, these three supramolecular systems exhibited slight influences on cell viability, indicating that all of them had good biocompatibility and low toxicity. As expected, C$_{60}$@(TPA-SP$_{PD}$⊂CB[8]) displayed good photodynamic activity at low concentration with white light irradiation (98.5% dead cells at 8 μM), which is attributed to the photoinduced ROS by the included C$_{60}$ (Fig. S45, ESI†). In other control groups, no obvious photodynamic activity was observed with light irradiation in TPA-SP⊂CB[8] or TPA-SP$_{PD}$⊂CB[8] (cell death with only 15.5% and 12.1%, respectively).

In conclusion, we have demonstrated a facile and bottom-up strategy to design a photoreaction-driven 2D polyrotaxane-type nanostructure through controlled non-covalent and covalent transformation in aqueous solution based on host–guest interactions. Benefiting from the intrinsic charge effect of CB[8], the obtained 2D periodic assembly maintained single-layer organization in both solution and solid states. More gratifyingly, the 2D periodic polyrotaxane-type assembly could be utilized as an efficient C$_{60}$ capture agent and then exhibit an excellent photodynamic therapy effect owing to the ROS production by the trapped C$_{60}$. It is envisaged that our strategy for developing 2D polyrotaxane-type nanoarchitectures can provide us with a convenient avenue for the creation of novel functional nanomaterials with good stability and biocompatibility.

We thank NNSFC (21432004, 21871154, 21772099, and 21861132001) for financial support.

Conflicts of interest

There are no conflicts to declare.

Notes and references

1 (*a*) J. W. Colson and W. R. Dichtel, *Nat. Chem.*, 2013, **5**, 453–465; (*b*) S.-L. Cai, W.-G. Zhang, R. N. Zuckermann, Z.-T. Li, X. Zhao and Y. Liu, *Adv. Mater.*, 2015, **27**, 5762–5770; (*c*) W. T. Dou, Y. Kong, X. P. He, G. R. Chen, Y. Zang, J. Li and H. Tian, *ACS Appl. Mater. Interfaces*, 2017, **9**, 14709–14715.
2 (*a*) K. S. Mali, J. Adisoejoso, E. Ghijsens, I. De Cat and S. De Feyter, *Acc. Chem. Res.*, 2012, **45**, 1309–1320; (*b*) S. Liu, J. Zhang, R. Dong, P. Gordiichuk, T. Zhang, X. Zhuang, Y. Mai, F. Liu, A. Herrmann and X. Feng, *Angew. Chem., Int. Ed.*, 2016, **55**, 12516–12521.
3 (*a*) K. Baek, G. Yun, Y. Kim, D. Kim, R. Hota, I. Hwang, D. Xu, Y. H. Ko, G. H. Gu, J. H. Suh, C. G. Park, B. J. Sung and K. Kim, *J. Am. Chem. Soc.*, 2013, **135**, 6523–6528; (*b*) Y. Li, Y. Dong, X. Miao, Y. Ren, B. Zhang, P. Wang, Y. Yu, B. Li, L. Isaacs and L. Cao, *Angew. Chem., Int. Ed.*, 2018, **57**, 729–733; (*c*) Y. Wang, Y. Kim and M. Lee, *Angew. Chem., Int. Ed.*, 2016, **55**, 13122–13126.
4 K.-D. Zhang, J. Tian, D. Hanifi, Y. Zhang, A. C.-H. Sue, T.-Y. Zhou, L. Zhang, X. Zhao, Y. Liu and Z.-T. Li, *J. Am. Chem. Soc.*, 2013, **135**, 17913–17918.
5 H.-L. Sun, Y. Chen, X. Han and Y. Liu, *Angew. Chem., Int. Ed.*, 2017, **56**, 7062–7065.
6 W. Z. Yuan, Y. Gong, S. Chen, X. Y. Shen, J. W. Y. Lam, P. Lu, Y. Lu, Z. Wang, R. Hu, N. Xie, H. S. Kwok, Y. Zhang, J. Z. Sun and B. Z. Tang, *Chem. Mater.*, 2012, **24**, 1518–1528.
7 J. Kim, I.-S. Jung, S.-Y. Kim, E. Lee, J.-K. Kang, S. Sakamoto, K. Yamaguchi and K. Kim, *J. Am. Chem. Soc.*, 2000, **122**, 540–541.
8 (*a*) H. Kashida, T. Doi, T. Sakakibara, T. Hayashi and H. Asanuma, *J. Am. Chem. Soc.*, 2013, **135**, 7960–7966; (*b*) R. Z. Lange, G. Hoger, T. Weber and A. D. Schluter, *J. Am. Chem. Soc.*, 2017, **139**, 2053–2059.
9 X. Tang, Z. Huang, H. Chen, Y. Kang, J. F. Xu and X. Zhang, *Angew. Chem., Int. Ed.*, 2018, **57**, 8545–8549.
10 H. Bakirci, A. L. Koner, T. Schwarzlose and W. M. Nau, *Chem. – Eur. J.*, 2006, **12**, 4799–4807.
11 T. Doi, H. Kashida and H. Asanuma, *Org. Biomol. Chem.*, 2015, **13**, 4430–4437.
12 M. Yamauchi, T. Ohba, T. Karatsu and S. Yagai, *Nat. Commun.*, 2015, **6**, 8936.
13 S. Liu, C. Ryspic, P. Mukhopadhyay, S. Chakrabarti, P. Y. Zavalij and L. Isaacs, *J. Am. Chem. Soc.*, 2005, **127**, 15959–15967.
14 T. Baati, F. Bourasset, N. Gharbi, L. Njim, M. Abderrabba, A. Kerkeni, H. Szwarc and F. Moussa, *Biomaterials*, 2012, **33**, 4936–4946.
15 Y. Liu, G.-S. Chen, Y. Chen, N. Zhang, J. Chen and Y.-L. Zhao, *Nano Lett.*, 2006, **6**, 2196–2200.
16 D. Chen and D. Sarid, *Phys. Rev. B: Condens. Matter Mater. Phys.*, 1994, **49**, 7612–7619.
17 J. Guo, Y. Xu, S. Jin, L. Chen, T. Kaji, Y. Honsho, M. A. Addicoat, J. Kim, A. Saeki, H. Ihee, S. Seki, S. Irle, M. Hiramoto, J. Gao and D. Jiang, *Nat. Commun.*, 2013, **4**, 2763.
18 Y. Chen, D. Zhao and Y. Liu, *Chem. Commun.*, 2015, **51**, 12266–12269.
19 (*a*) X. Wang, C. X. Yang, J. T. Chen and X. P. Yan, *Anal. Chem.*, 2014, **86**, 3263–3267; (*b*) Z.-Q. Li, Y.-M. Zhang, D.-S. Guo, H.-Z. Chen and Y. Liu, *Chem. – Eur. J.*, 2013, **19**, 96–100.